



A comparison of gear tooth bending fatigue lives from single tooth bending and rotating gear tests

Isaac Hong¹ · Zach Teaford¹ · Ahmet Kahraman¹

Received: 25 March 2021 / Accepted: 21 June 2021 / Published online: 13 September 2021
© Springer-Verlag GmbH Deutschland, ein Teil von Springer Nature 2021

Abstract

Gear tooth bending fatigue failures are instantaneously catastrophic to gear drive power transmission systems. For this reason, gear designers must understand the limits of their design with respect to the desired application and service time. Fatigue testing on gear specimens has been preferred metric on which to base future designs. Single Tooth Bending test (STB) or a Rotating Gear (RG) test methodologies have been used for this purpose. STB type tests generally form the large majority of gear fatigue testing due to cost and availability but does not fully simulate the actual operating conditions of rotating gears in service. As RG evaluations are costly and time-consuming, it is desirable to quantify how a stress-life (SN) relationship regressed through STB testing compares to that produced in RG testing. In this study, both STB and RG test methodologies are employed to test the same specimen design. Matrices of fatigue tests are executed and statistical regression techniques are used to estimate bending fatigue lives as a function of stress for both sets of data. The resultant SN curves are compared to determine any differences in allowable stress. Techniques are then employed using single set data (STBF or RG individually) to demonstrate the calculation of correlation coefficients, which can approximate the total difference determined between the two data sets.

Ein Vergleich der Ermüdungserscheinungen von Zahnradzähnen aus Einzelzahnbiege- und Drehgetriebetests

Zusammenfassung

Ermüdungsfehler der Zahnzahnbiegung sind augenblicklich katastrophal für Getriebeantriebssysteme. Ermüdungsprüfungen an Verzahnungsproben wurden für zukünftige Konstruktionen bevorzugt. STB-Baumusterprüfungen bilden in der Regel aufgrund der Kosten und der Verfügbarkeit die überwiegende Mehrheit der Getriebeermdungsprüfungen, simulieren aber nicht vollständig die tatsächlichen Betriebsbedingungen rotierender Zahnräder im Betrieb. In dieser Studie werden sowohl STB- als auch RG-Testmethoden verwendet, um dasselbe Probedesign zu testen. Die resultierenden SN-Kurven werden verglichen, um eventuelle Unterschiede in der zulässigen Spannung zu bestimmen. Techniken werden dann unter Verwendung einzelner gesetzter Daten (STBF oder RG einzeln) verwendet, um die Berechnung der Korrelationskoeffizienten zu demonstrieren, die die Gesamtdifferenz näherungsweise bestimmen können, die zwischen den zwei Datensätzen bestimmt wird.

Abbreviations

Availability of data and material The authors testify that all supporting data is included.

Code availability Not applicable

Consent to participate Not applicable.

Consent for publication All authors consent to the publication of this work.

✉ Isaac Hong
hong.250@osu.edu

¹ Gear and Power Transmission Research Laboratory,
Department of Mechanical and Aerospace Engineering, The
Ohio State University, Columbus, OH 43210, USA

B_{50}	50% failure rate
f	fatigue test frequency
f_s	number of surface initiated failures
f_{ss}	number of subsurface initiated failures
F	STBF test applied force
K_d	dynamic factor
K_f	initiation location factor
K_S	statistical factor
K_{RS}	total RG to STB factor
K_F	loading factor
K_R	stress factor
N	number of cycle in a test
N_f	number of cycles to failure
N_{if}^s	number of cycles to failure for a surface initiated specimen
N_{if}^{ss}	number of cycle to failure for a subsurface initiated specimen
p	failure percentile
q_{RG}	failure percentile of teeth on a RG specimen
r_f	ratio of surface initiated to total number of failures
R	fatigue test stress ratio
α_1	regressed intercept constant
α_2	regressed slope constant
β_1	regressed variance constant
γ	regressed fatigue strength constant
σ_a	stress amplitude
σ_m	stress mean
σ_{ult}	ultimate tensile stress
σ_{fat-RG}	fatigue strength from RG test
$\sigma_{fat-STB}$	fatigue strength from STBF test
$\bar{\sigma}_g^{f=0}$	measured gage stress at 0Hz
$\bar{\sigma}_g^{f=40}$	measured gage stress at 40Hz
$\bar{\sigma}_{max}$	normalized maximum gear tooth root bending stress
$\bar{\sigma}_{RG}^{(p)}(N_f)$	RG SN curve at specified failure percentile
$\bar{\sigma}_{STB}^{(p)}(N_f)$	STB SN curve at specified failure percentile

1 Introduction

The durability and life of gears is critical to the safe operation of power transmission systems they are used in. Long life of these components reduces costs associated with maintenance, repair, and warranty. One well known failure mode of gears is tooth root bending fatigue. This failure mode is the result of two main operating principles of gears. The first, is that gear teeth act as cantilever beams when supporting load. This creates a stressed volume at the root, which is a function of the applied load and root geometry. Secondly, the gear tooth is loaded only while in mesh and is in a relaxed state outside the mesh, producing cyclic

stress states in the gear teeth roots where the frequency of loading is dependent on gear rotational speed and kinematic configuration of the gear train.

Gear tooth bending fatigue is a catastrophic failure where almost instantaneously the load carrying capacity of the gear is extinguished as one tooth is separated and poor meshing conditions cascades the failure to the rest of the gear teeth. In order to prevent this failure, gear designers must either have an accurate set of predictive failure models or extensive experimental data, else revert to overly large factors of safety producing heavy and costly designs that may underperform. The current state of available predictive models for high cycle or very high cycle gear tooth bending fatigue failure is limited. The most sophisticated models employ a form of multiaxial fatigue criteria of which there are many with no consensus on their accuracy with respect to gear tooth bending fatigue. These models still rely on empirical interpretations of experimental material fatigue data. Due to the uncertainty of these models, gear designers still many times rely on experimental gear tooth bending fatigue data.

The preferred experimental data for gear designers comes from direct testing on gear specimens either in the form of single tooth bending fatigue methodologies (STBF) or rotating gear (RG) methodologies. STBF is by volume the large majority of gear tooth bending fatigue testing performed. Many adaptations can be found in literature either using specialty anvils to contact a fixed gear or using a mating gear to apply load to a fixed gear in a specific position [1–27]. By comparison, very few examples of RG testing exist [2, 6, 16, 23, 27–32]. Many early studies had mixed results with multiple modes of failure and extensive damage to the gearbox upon tooth failure. However, recent studies by Winkler et al. [2], Hasl et al. [32] and Hong et al. [29, 33] highlight the feasibility of RG testing as a reliable methodology for gear tooth bending fatigue testing.

There is a need to improve upon the understanding of how STBF test results compare to the expected life of a production gear designed based on available STBF data and the results of RG testing in order to unify data sets. Four main differences between rotating and single tooth bending must be reconciled in order to understand the comparison in fatigue life between RG and STB gear tooth bending fatigue testing.

1. The first difference in fatigue life due to harmonic loading vs gear mesh loading condition along with different test frequencies. This was discussed in ref [33]. but no empirical or physical relationship was offered. In STBF testing, a sinusoidal cyclic load is applied to a single gear tooth producing a proportional sinusoidal stress in the loaded gear tooth root. In a loaded gear mesh any given tooth is loaded only during the short period it meshes

- with a tooth of the mating gear and is unloaded during the rest of the rotation. The load distribution that the tooth experiences is then a function of the tooth geometries, hub, web and rim compliances, and operating conditions. For a single parallel axis spur gear pair with a relatively stiff hub, web and rim, this means that gear tooth root stress is zero for $100(z-\varepsilon)/z$ percent of the loading cycle where the loading cycle length is equivalent to one rotation of the gear, z is the number of teeth on the gear and ε is the operating profile contact ratio. The effect of the zero stress relaxation period as well as the difference in loading form on fatigue life is unknown. Limited studies [34, 35] on the effect of frequency and load shape has been done on notched specimens but within the context of corrosion prone environments, making their applicability to gear fatigue unknown.
2. The second difference is the statistical difference in fatigue life due to definition of the specimen. This difference was first mentioned by Seabrook and Dudley [23] in 1964. In RG testing, the specimen is the entire gear. Failure of the specimen constitutes one tooth failing and suspension of the remaining $z-1$ teeth. In STBF testing, the specimen is a single tooth on a gear. Multiple teeth can be tested on a single gear and each tooth tested either fails or suspends. A mathematical relationship to describe this statistical difference was suggested by McPherson and Rao [6] but no conclusive evidence to its validity was found. This also raises the question of manufacturing variation effect differences between STBF and RG testing. It is plausible that for any single gear, machining and processing variation magnitudes may be smaller than comparing between different gears. It is also possible to perform an entire matrix of STBF testing from a single gear while RG testing must always involve multiple gear specimens to create statistical conclusions. Larger standard deviations may therefore be expected from RG testing. The statistical difference between computing median fatigue life from individual tooth failures and suspensions to the life computed from entire gear failures must be accounted for.
 3. The third difference is the achievable stress ratio or ratio of the minimum to maximum load. This difference was also discussed by McPherson and Rao [6]. Fully reversed stresses have a stress ratio $R = -1$ as the compressive stress achieved in each cycle is equal and opposite the tensile stress. Fully released stress ($R = 0$) achieves a minimum stress of exactly zero in each stress cycle. STBF testing is generally limited to $R > 0$. $R = 0$ ratios are not used in STBF testing to avoid impact at the tooth contact interface. In addition, creating $R < 0$ ratios in a STBF test requires a non-parallel loading axis and additional support adding extreme complexity to a space constrained test setup. RG testing on the other hand is generally limited to $R \leq 0$ ratios as all the gear teeth experience an unloaded state out of mesh constraining the minimum achieved root stress to zero or less than zero in idler and planet configurations. This means that there is no single stress ratio that both STBF and RG testing can achieve. However, the fact that stress ratio has an effect on fatigue life is very well documented dating back to the 1873 works of Müller [36] through arguably more well-known from contributions by Goodman [37]. It is worth noting that in some high-speed applications, the minimum gear tooth root stress ratio is greater than zero representing a baseline non-zero tensile root stress when the gear teeth are not in mesh. This is generated from centrifugal forces expanding the rim of the gear creating tensile hoop stresses and the effect of the gear teeth pulling outward from the rim. However, no RG test setup currently exists to perform controlled $R > 0$ bending fatigue tests.
 4. Final major difference is the potential for different crack initiation locations. A crack initiation in gear tooth bending fatigue can be categorized as either surface or sub-surface. Surface cracks are thought to be initiated from local stress concentrations created from small radii in the machine tooling such as cutters and grinders [38]. Sub-surface initiations originate from non-metallic inclusions such as sulfides, oxides and silicates or from voids in the material microstructure [39]. These subsurface locations are still very close to the surface (<0.1 mm deep) and have very distinct optical characteristics usually described as a “fisheye” [40]. It has been empirically found that the fatigue lives associated with these two initiation locations are different with sub-surface initiations being described as having longer fatigue lives for any given finite life producing stress level. This empirical finding has given rise to the step-wise SN curve [40]. Therefore, fractographic images should be taken from failure surfaces to ensure correct categorization and separation of data sets. Furthermore, initial evidence from RG and STBF testing by Winkler et al. [2] suggests that STBF and RG testing tend to produce failures of opposite initiation type with the STBF testing producing more surface initiated cracks and RG testing producing more sub-surface initiated cracks though this behavior may be somewhat material/processing related as well. Both initiation types have been observed in both STBF and RG testing.
- The scope of developing robust empirical relationships reconciling all of these differences is difficult. This is further complicated by the uncertainty that the relationship will be equivalent for different materials and material processing methods such as surface hardening methods, peening and surface roughness processing. The statistical difference has been partially explored by Seabrook and Dudley [23]

and more recently McPherson and Rao [6]. Seabrook and Dudley found an approximate 30% increase in the fatigue strength estimated from STBF tests as compared to a limited number of RG tests. They attributed the difference to dynamic loading in the RG test but made note that failure in the RG tests is represented by the weakest tooth on the gear. McPherson and Rao [6] calculated an adjusted normal probability variant to account for the probability of one tooth failing on a gear of z teeth. This adjusted normal probability variant was then used to adjust the fatigue strength calculated from binary pass/fail STBF data at various loads to an equivalent RG fatigue strength. Calculated fatigue strengths were compared to a limited set of RG data and found to be significantly less than the experimental data suggests with select data points showing closer agreement. This methodology also included a formulation for accounting for stress ratio differences in the STB and RG data by using known empirical relationships for constant life similar to Goodman/Haigh to compute equivalent stresses at a different stress ratio for equivalent fatigue life or at the fatigue strength. McPherson and Rao [6] also noted that the experimental STBF and RG data generated as part of the study showed approximately a 30% increase in estimated fatigue strength, consistent with finds by Seabrook and Dudley [23].

A single empirical fraction of $\sigma_{\text{fat-RG}} = 0.9\sigma_{\text{fat-STB}}$ translating the estimated fatigue strength from STBF testing to RG testing and assumed to be accounting for all four of the above mentioned test differences is also given in several manuscripts [2, 14, 16, 19]. The empirical origins of this transformation constant appear to be from a statistical report of Forschungsvereinigung Antriebstechnik (FVA) Project 304 in 1999 [16, 41] or earlier origins in a 1987 German manuscript by Rettig [42] or both. Both manuscripts are only available in German making their review in the English context difficult.

As described, the existing technology pertaining to the translation of STBF to RG bending fatigue testing is limited. Even with availability of the previously mentioned German works, it is still limited to comparing the assumed fatigue strength. Contemporary work suggests that very high cycle fatigue (VHCF, $N_f > 10^7$) lives of sub-surface initiated cracks in certain materials or materials of certain microstructure formations may not exhibit conventional endurance limit/fatigue strength behavior [43]. As longer service life of machines is desirable, the expected service life of a gear will need to keep pace with other components. Therefore, it becomes increasingly necessary to develop robust empirical relations between the vast existing body of STBF data to limited high cycle fatigue (HCF, $10^3 > N_f > 10^7$) and VHCF RG data. Accordingly, The goals of this research are to (i) demonstrate a unified methodology of STBF and RG testing on a single test

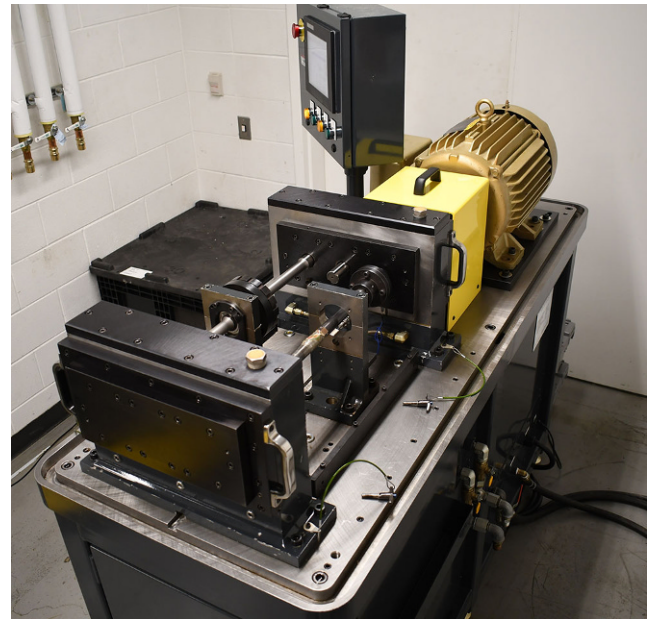


Fig. 1 A three axis rotating gear fatigue test machine

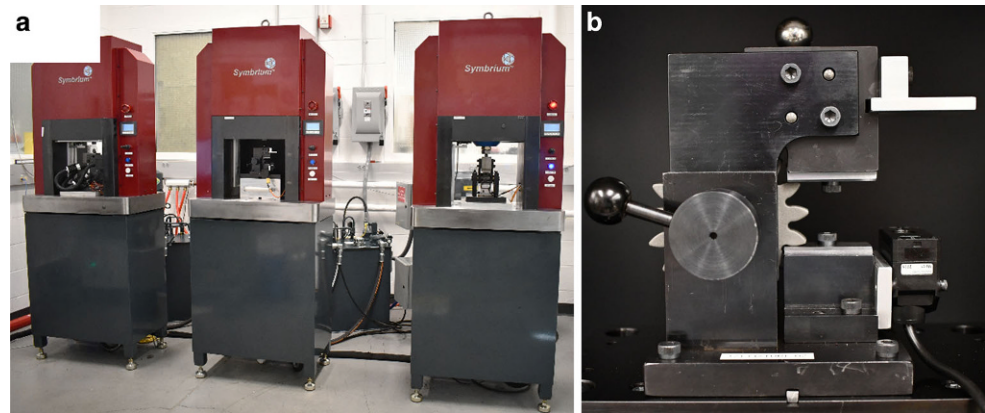
specimen, (ii) investigate statistical techniques that can be used consistently for both STBF and RG testing in order to regress Stress-Life (SN) relationships, (iii) define empirical relationships using single set data (STBF or RG only) which allow for the estimation of the total STBF to RG difference based on the four individual differences described above, and (iv) add empirical data to the existing limited STBF vs RG test datasets.

2 Experimental setup

2.1 Rotating gear test

An existing RG test methodology by Hong et al. [29, 30] was adopted in order to perform HCF and VHCF gear tooth bending fatigue testing at a stress ratio of $R = 0$. It consisted of a 91.5 mm center distance power circulating (back-to-back) test machine featuring three axes of rotation. Modular connections among the three axes and between the two gearboxes allowed for the application of various gear tooth loading types including idler (fully reversed stress) loading and torque split (sun gear type) loading. In its simplest form the machine was reduced to a two-axis arrangement with a single gear pair in each gearbox producing fully released ($R = 0$) gear tooth root stresses. A split coupling was used to apply a constant torque to the gears and an external AC motor drives the power circulating loop. Fig. 1 shows an image of one of several identical RG fatigue test machines used in this investigation.

Fig. 2 a A STB fatigue test load frames, and b STB test fixture



Lubrication and heat removal were accomplished via a liquid-cooled oil bath. Vibration based algorithms monitored test activity and shutdown the test at the onset of tooth fracture, capturing the failure with a macro surface crack sustained from the application of plastic strains at the crack tip but prior to complete separation of the gear tooth. Rotation speed of the test pinion was sustained at about 4400rpm for all load levels used in testing. Dynamic strain measurements performed on the gearbox at test load and speed conditions yielded dynamic root stress factors K_d of about 0.94–0.99 depending on load. These dynamic factors were accounted for in the reported stresses for the RG testing.

The gear pair used in the RG test setup consisted of a 17T pinion and a 25T gear where the 17T pinion was engineered to fail exclusively from tooth root breakage. Contact stresses were kept modest and an ISO 150 lubricant was used to minimize the effects of wear. Temperatures were sustained at 90°C throughout the duration of the test. When the machine was utilized with three axis, a second 25T gear was used with the 17T acting as the central idler member.

2.2 Single tooth bending fatigue test

A STBF fixture was designed and fabricated for the testing of the RG test specimen. The setup was made to be compatible with a series of universal hydraulic oscillators located at The Ohio State University and shown in Fig. 2a. These hydraulic oscillators were capable of applying a 130kN maximum force with oscillation frequencies peaking around 100Hz.

In a STB test, the desired load path is for force to travel through the upper anvil through the test tooth and be reacted only by the reaction tooth supported by the lower anvil. In order to achieve this the gear must be in static equilibrium from the test tooth and reaction tooth forces. As these forces result in line contact in a spur gear, the contact lines must be parallel, and the test and reaction contact surfaces must

also be parallel. The contact locations such that these criteria were satisfied were determined. While multiple sets of contact points exist which satisfy the prior described conditions, the contact point was designed to be approximately the highest point of single tooth contact (HPSTC) in the RG test setup. These STBF fixtures utilize a fixed lower anvil which support the reaction tooth. The test gear is then located via a centering shaft with soft oil impregnated bronze acting as a bushing between the test gear inner diameter and the locating shaft. An upper anvil is aligned via the same centering shaft such that the upper anvil contacts another gear tooth (test tooth) at a contact point in the addendum. A ball bearing is used between the ram and the fixture to negate effects of small amounts of misalignment between the axis of the ram and the desired axis of the load path. An image of an assembled test fixture is shown in Fig. 2b.

Tooth root strain measurements were taken in order to validate the fixture design and stress prediction models. A finite element based tooth root stress prediction solver as part of a gear tooth load distribution model [44] was used to predict the state of stress in the test tooth root based on the loading position defined in above. Strain gauges were mounted in the root of a 17T gear specimen at the predicted location of maximum tooth root stress. Two sets of loaded strain measurements were recorded. The first was a dy-

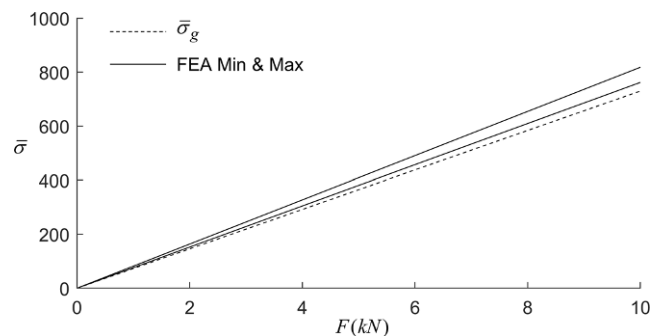


Fig. 3 Comparison of measured and FEA predicted STBF tooth root stress

dynamic cycling of the test tooth in order to measure strains under conditions similar to the fatigue test. Lower loads were used in order to avoid exceeding the fatigue strength of the strain gauge but the fatigue test operating frequency of 40Hz and a stress ratio of $R = 0.05$ was used. The second was a quasi-static measurement where load applied to the gear test tooth was increased at a steady-state condition. First, the stress maximums achieved in each cycle under dynamic conditions were compared to the equivalent bending stress produced under quasi static conditions at equivalent load set-points F in order to evaluate if any dynamic effects were present. A dynamic factor was calculated as

$$K_d = \frac{\frac{1}{N} \sum \max(\bar{\sigma}_g^{f=40})_k}{\bar{\sigma}_g^{f=0}(F)} \tag{1}$$

Where $\bar{\sigma}_g^{f=0}(F)$ is the normalized measured gage stress under quasi-static conditions at loading frequency $f = 0$, and $\max(\bar{\sigma}_g^{f=40})_k$ is the maximum normalized measured gage stress corresponding to the k^{th} cycle at a loading frequency of 40Hz. At all loading conditions tested, $0.99 \leq K_d \leq 1.01$ indicating very minimal dynamic effects.

The measured gage bending stresses were also compared to the predicted tooth root stresses. As the strain gage has non-zero area, it cannot measure at a singular point as in FEA analysis. Therefore, the minimum and maximum FEA stress within the footprint area of the strain gage was com-

pared to the measurement shown in Fig. 3. The measured gage stresses are shown to be slightly lower than the FEA but are still very reasonable. Possibilities for the error are in gage placement where very small placement errors may result in large changes in measured stress. Overall, the measurement shows that STB fixture is performing as designed.

3 Fatigue tests and results

A series of tests were performed utilizing the RG test setups in the two-axis ($R = 0$) arrangement as well as on the STB test setups. A batch of equivalent case-carburized test gears made of high-end alloy gear steel were procured for this testing. Tables 1 and 2 show the results of RG and testing and STB tests, respectively. A SN plot showing the both sets of data married together is shown in Fig. 4. The maximum bending stress values for both test results have been normalized for confidentiality reasons and are denoted as $\bar{\sigma}_{max}$.

It is important to note what was and was not included in the SN curve of Fig. 4 with respect to the four differences in testing described in the introduction. Specifically, no corrections were made (i) to account for differences in the loading form, (ii) to account for the difference in test specimen identification, (iii) to explain the difference in the stress ratio where the RG testing is performed at $R = 0$ and the STB testing is performed at $R = 0.05$, and (iv)

Table 1 RG Test Results

$\bar{\sigma}_{max}$	N_f (M)	Result
344	200	Runout
400	100	Runout
477	50	Runout
477	100	Runout
477	150	Runout
477	150	Runout
518	100.9	Failed
518	16.7	Failed
518	25.7	Failed
518	34.2	Failed
518	37.2	Failed
518	65.3	Failed
579	0.233	Failed
579	0.242	Failed
579	0.321	Failed
579	25.9	Failed
579	26.2	Failed
579	60.1	Failed
649	0.189	Failed
649	11.2	Failed

Table 2 STB Test Results

$\bar{\sigma}_{max}$	N_f (M)	Result
521	10	Runout
521	10	Runout
558	10	Runout
558	0.236	Failed
595	10	Runout
595	0.058	Failed
595	8.18	Failed
670	10	Runout
670	0.066	Failed
670	0.067	Failed
670	0.111	Failed
670	0.684	Failed
745	0.019	Failed
745	0.049	Failed
745	0.459	Failed
745	5.1	Failed
745	0.031	Failed
763	3.45	Failed
782	0.054	Failed
819	0.021	Failed
819	0.034	Failed
894	0.019	Failed

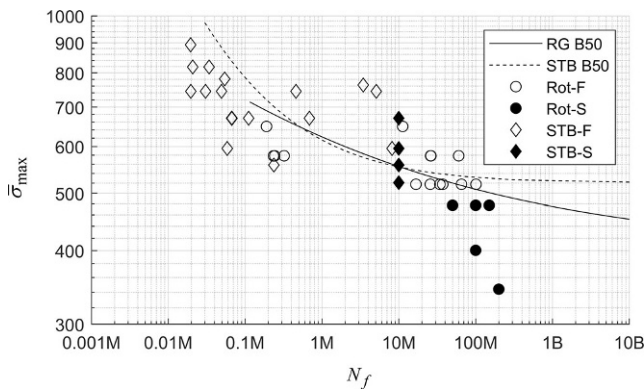


Fig. 4 RG and STB fatigue test results along with the regressed median fatigue lives for each population

to account for potential differences in crack initiation location differentiating between surface and subsurface failure modes.

The total difference between the STB and RG testing will first be quantified without any corrections. Following that quantification, methods to derive individual differences from a single set of data only will be demonstrated and the aggregate total of those errors will be shown to closely estimate the total difference.

3.1 Data analysis

The SN plot of Fig. 4 visualizes the difference between RG and STB testing accounting for all four of the differences described. This total difference percentile K_{SR} can be described as

$$K_{RS}(N_f) = \frac{\bar{\sigma}_{RG}^{(p)}(N_f)}{\bar{\sigma}_{STB}^{(p)}(N_f)} \tag{2}$$

where $\bar{\sigma}_{RG}^{(p)}(N_f)$ is the SN relationship between the stress parameter $\bar{\sigma}$ and the failure life N_f regressed from the rotating gear testing for a failure percentile of p . Correspondingly $\bar{\sigma}_{STB}^{(p)}(N_f)$ is the equivalent for STB testing. As the slopes between $\bar{\sigma}_{RG}^{(p)}(N_f)$ and $\bar{\sigma}_{STB}^{(p)}(N_f)$ may not be equal, K_{RS} is therefore a function of N_f as well. K_{RS} comprises of the four differences between RG and STB testing. It can therefore be described as the product of the difference in allowable stress for equivalent fatigue lives from each individual source.

$$K_{RS} = K_F K_S K_R K_I \tag{3}$$

where K_F is the difference in allowable stress for equivalent fatigue lives between RG and STB testing due to differences in the applied force time history alone. K_S accounts for the shift in SN relationships due to statistical differences derived from specimen definition, K_R is the difference in SN

relationships due to differences in test stress ratio R , and K_I accounts for the SN differences associated with varying crack initiation locations. Each of these factors relates to physical difference in the fatigue testing but mathematical or empirically validated relationships for these physical parameters do not exist.

Knowledge of the total scaling factor K_{RS} for one set of testing does not guarantee congruency with testing from other gear designs, materials and test methodologies. The statistical difference parameter K_S will change if the tooth count of the RG specimen changes as more teeth are simultaneously cyclically loaded with higher tooth counts. Different test methodologies may employ different stress ratios in the STB testing requiring a change to only the stress ratio parameter K_R . In addition, different materials may have different constant life (Goodman) relationships which varies K_R even for the same stress ratios. K_I , in addition, may be influenced by material changes where the ratio of subsurface and surface initiated failures from RG and STB testing may be material influenced. Failure to account for any of these parameters may lead to poor correlation between RG and STB data sets.

It would be extremely beneficial to the knowledge base to determine empirical or physical relationships for each of the four parameters, K_F , K_S , K_R , and K_I . However, large databases of RG and STB data would be needed for validation. The current study will use the limited data shown in Tables 1 and 2 and Fig. 4 to demonstrate techniques to derive the total difference and suggest methods of determining the statistical parameter K_S and the stress ratio parameter K_R .

3.2 Stress-life regression

The Stress-Life relationships $\bar{\sigma}_{RG}(N_f)$ and $\bar{\sigma}_{STB}(N_f)$ are determined using Maximum Likelihood Estimates (MLE). The statistical likelihood that the experimental results shown in Fig. 4 occur is computed by assuming a general form of $\bar{\sigma}_{max}(N_f)$ and also assuming a distribution for which N_f varies at any given stress level $\bar{\sigma}_{max}$. The solution for the parameters describing the distribution (i.e. mean and standard deviation for a Gaussian distribution) and the assumed form of the $\bar{\sigma}_{max}(N_f)$ relationship (i.e. m and b for a linear relationship of form $\sigma = mN_f + b$) for which the likelihood is maximized. This set of parameters which maximize the likelihood are then said to be the optimal solution for the assumed SN relationship and distribution. In practical implementation the median or B_{50} percentile survival value $B_{50} = \bar{\sigma}_{max}^{50}(N_f)$ is set to be equal to the functional SN relationship. The standard deviation or other distribution descriptive parameters may be constants or also functional relationships of stress or life. In addition, the regression assumes life is the random variable and must be performed as $N_f(\bar{\sigma}_{max})$.

Table 3 SN Regression Parameters

	α_1	α_2	γ	β_1
RG	47,906	-6.307	400.6	0.599
STBF	24,156	-2.264	519.2	0.833

The assumed form of the SN relationship and statistical distribution are at the discretion of the analyst. As almost any form can be used, it is important to note that correlation \neq causation and the seemingly best fitting relationships may not represent the physics of the fatigue process. A regression suggested by Pascual and Meeker [45] utilizing an assumed function with a regressed horizontal asymptote representing a fatigue strength will be used here to compute SN relationships for both the STB and RG data. The median Life-Stress relationship is defined as

$$N_f^{50}(\bar{\sigma}_{\max}) = \alpha_1 + \alpha_2 \ln(\bar{\sigma}_{\max} - \gamma), \quad \min[(\bar{\sigma}_{\max})_{if}] > \gamma \tag{4}$$

where α_1 and α_2 are regressed constants related to the y-intercept and slope and γ is a regressed fatigue strength which must be less than lowest cyclic stress level producing failure $[(\bar{\sigma}_{\max})_{if}]$ and if is an index of fatigue test stress levels producing failure. A log-normal distribution is assumed to describe the fatigue life distribution at any given stress level yielding the general form of the regression for a failure rate of q percent to be

$$N_f^q(\bar{\sigma}_{\max}) = N_f^{50}(\bar{\sigma}_{\max}) + z e^{[\beta_1]}, \quad \min[(\bar{\sigma}_{\max})_{if}] > \gamma \tag{5}$$

where β_1 are regressed constants related to variance. z is the standard normal variate corresponding to the q th percentile. Both the assumption of a fatigue limit in STB and RG gear tooth bending fatigue data and that the life distribution follows a lognormal distribution are commonly used in literature [46]. Table 3 provides the regressed parameters $\alpha_1, \alpha_2, \beta_1$ and γ for both the RG and STB testing. Also

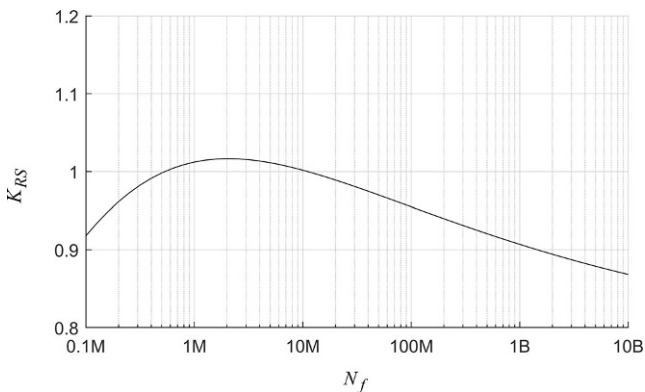


Fig. 5 Total ratio of stresses at equivalent fatigue lives between RG and STB testing

shown in Fig. 4 are both SN regressions plotted for a range corresponding to 90% of the minimum stress run in the corresponding test type up to 110% of the maximum stress run. A close agreement between the two regressions is observed, indicating that the total difference percentile K_{RS} is close to unity within the range plotted. K_{RS} is computed according to Eq. (2) using the B_{50} life such that

$$K_{RS}(N_f) = \frac{\bar{\sigma}_{RG}^{50}(N_f)}{\bar{\sigma}_{STB}^{50}(N_f)} \tag{6}$$

and is plotted in Fig. 5. Two points are of particular interest from Fig. 5. First, the ratio of the regressed fatigue strengths is shown as the asymptotic behavior of the regression produces a constant as $N_f \rightarrow \infty$ and as expected the RG fatigue strength is lower than the STB fatigue strength. This behavior will be investigated more in the context of removing the effect of the four individual physical differences individually. Secondly the ratio increases as N_f nears 1M and even indicates that the RG life is longer than corresponding STB lives. Below about 1M cycle life range the ratio then decreases again indicating that cyclic stresses will be lower for RG testing when producing fatigue lives closer to representing low cycle fatigue behavior. However, it is anticipated that this ratio will not be constant for all RG to STB test comparisons. Rather, mathematical or empirical relations must be developed to broaden the utility of this RG to STB comparison formulation.

3.3 Statistical factor K_s

As it is more useful to convert STB data to an RG equivalent, a possible formulation for doing so will be provided. The basis for this is the regression of the log-normal variance completed as part of the full regression of Sect. 3.2. As the test gear specimen has 17 teeth, the STB data needs to be converted to an equivalent 1:17 failure rate. This corresponds to a standard normal variant of $z = -1.5647$. Eq. (5)

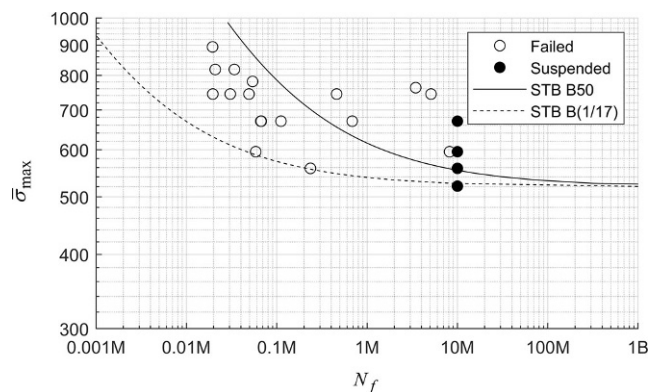


Fig. 6 STB B50 fatigue lives compared to STB B(1/17) fatigue lives

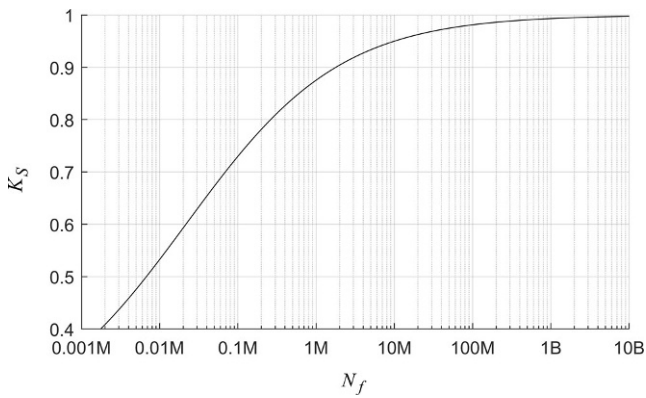


Fig. 7 Ratio of bending stresses between RG and STBF testing due to statistical differences

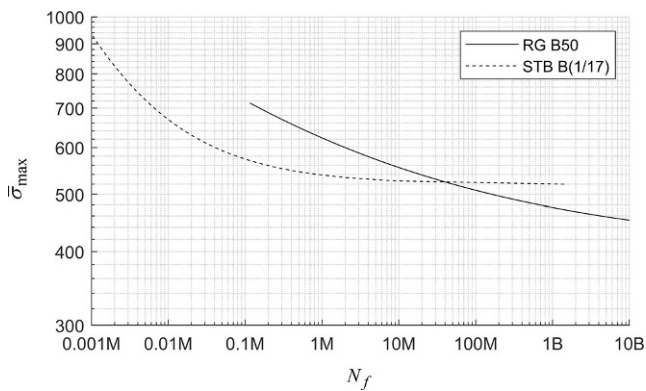


Fig. 8 RG B50 fatigue lives compared to STB B(1/17) fatigue lives

is then used to compute $N_f^{1/17}(\bar{\sigma}_{max})$. A comparison of $N_f^{50}(\bar{\sigma}_{max})$ and $N_f^{1/17}(\bar{\sigma}_{max})$ for the STB data is shown in Fig. 6. I shows that at the $q = 1/17$ percentile is shifted to the left and has a constant variance as indicated in Eq. (5). It also lacks any significant difference in the regressed fatigue limit. Let q_{RG} be the failure percentile corresponding to the number of teeth failed versus the number of teeth z_p on a RG test specimen. Assuming one tooth fails in an RG test,

$$q_{RG} = \frac{1}{z_p} \tag{7}$$

and the statistical coefficient K_S can be defined as

$$K_S = \frac{\bar{\sigma}_{STB}^{(q_{RG})}(N_f)}{\bar{\sigma}_{STB}^{(50)}(N_f)} \tag{8}$$

A plot of K_S is shown in Fig. 7. K_S is between 0.53 and 0.99 at reasonable life ranges corresponding to the tested life. The RG $N_f^{50}(\bar{\sigma}_{max})$ is then compared to the STB $N_f^{q_{RG}}(\bar{\sigma}_{max})$ in Fig. 8. This plot is the equivalent of

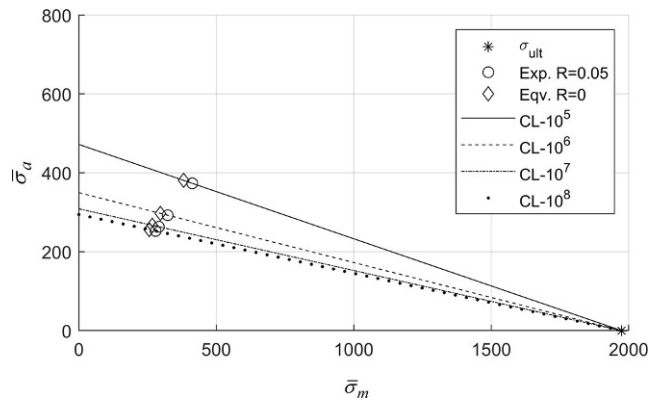


Fig. 9 Constant Life Diagram showing STB R=0.05 stress and comparable STB R=0 stresses

$$K_S \bar{\sigma}_{STB}(N_f) = \bar{\sigma}_{RG}(N_f) \tag{9}$$

where K_F , K_R , and K_I are missing. It is noted that although Fig. 8 might indicate further separation of the RG and STB regressions, this phenomena is commonly observed in very high cycle fatigue corresponding to separation of SN curves between surface failures and subsurface failures. These separate curves are also referred to as Step-wise SN curves [40]. Therefore, it is reasonable to suggest that including a factor accounting for the difference in the SN curves from surface failures and subsurface failures would then bring the difference in the final observed test data back to almost one. This further suggests that the effects of K_F and K_R may be minimal.

3.4 Stress ratio factor K_R

Equivalent stresses at different stress ratios for constant life (CL) is a long studied phenomenon as discussed in the introduction by researchers such as Müller, Goodman and many others. These constant life relationships are dependent on material and should therefore be evaluated individually.

An ultimate tensile strength test was completed on the gear test specimen using the STB test machine. Load was slowly applied on an unused tooth until failure. The peak load sustained was recorded and associated tooth root bending stresses were computed. It was found that the ultimate tensile strength of the gear tooth in bending was $\bar{\sigma}_{ult} = 1967$. A repeat test resulted in less than 0.7% difference in $\bar{\sigma}_{ult}$.

The modified Goodman approach was then be used to determine the effect where for tensile mean stresses

$$\sigma_a = \frac{-\sigma_{R=-1}}{\sigma_{ult}} \sigma_m + \sigma_{R=-1} \tag{10}$$

where σ_a and σ_m are alternating and mean stresses respectively and $\sigma_{R=-1}$ is the fully reversed cyclic stress amplitude

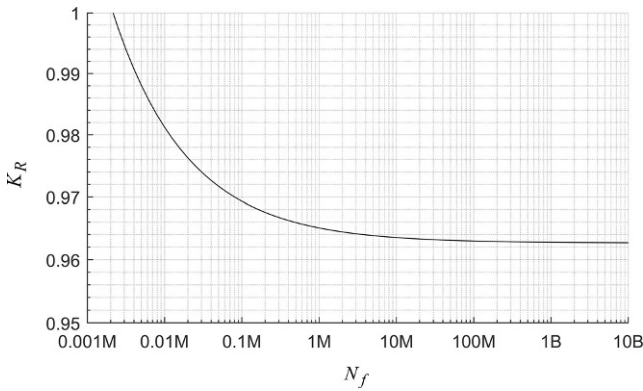


Fig. 10 Stress ratio factor K_R

corresponding to equivalent fatigue life. Eq. (10) defines a line of constant life for all stress ratios $-1 \leq R < 1$ producing $\sigma_m \geq 0$. In this work the mean and amplitude cyclic stress producing any given fatigue life is known at a stress ratio of $R = 0.05$ along with $\bar{\sigma}_{ult}$. The RG testing produced a stress ratio of $R = 0$. Therefore $\sigma_{R=0}$ can be solved for any N_f using the STB data and using $\bar{\sigma}_{ult}$. An equivalent σ_a , σ_m and σ_{max} can then be computed corresponding to a stress ratio of $R = 0$ by converting the STB data to an equivalent stress ratio as the RG data. The constant life map showing the solution for Eq. (10) as well as the converted STB data for lives of $N_f \in [10^5, 10^6, 10^7, 10^8]$ is shown in Fig. 9. K_R can then be defined as

$$K_R = \frac{\bar{\sigma}_{STB}^{(R_{RG})}(N_f)}{\bar{\sigma}_{STB}^{(R_{STB})}(N_f)} \tag{11}$$

where $\bar{\sigma}_{STB}^{(R_{RG})}(N_f)$ is the STB SN relationship converted to a equivalent stress ratio as the RG data R_{RG} . This technique can be used for other stress ratio conversions beyond the $R = 0.05$ to $R = 0$ as demonstrated here. K_R is plotted in Fig. 10. It is observed that the maximum stresses at $R = 0$ are within about 96% to 99% of the equivalent maximum

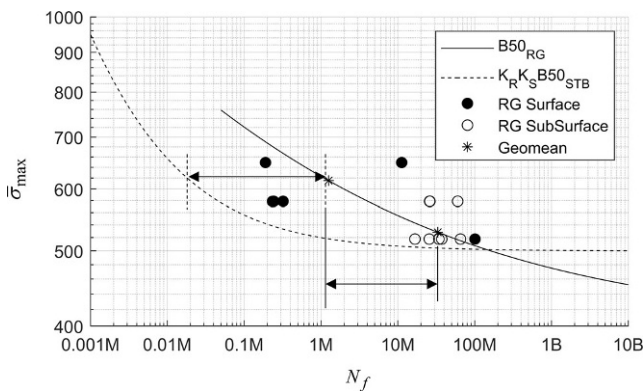


Fig. 11 Comparison of RG surface initiated failures and RG subsurface initiated failures

stress at the STB test stress ratio of $R = 0.05$. This indicates that the difference in STB and RG testing resulting only from stress ratio testing differences in STB and RG testing is much less than the statistical difference K_S .

3.5 Initiation location factor K_I

The difficulty in determining the difference in SN relationships due to surface and subsurface initiation differences is shear quantity of data. In order for this to produce a statistically conclusive difference, a single testing program (RG or STB) would need to generate sufficient data containing both surface and subsurface failures to regress both independently. A full statistical analysis between the two sets is beyond the capabilities of the current data set. However, simplified measured to estimate the difference may still be employed.

Fractographic inspections were performed on the RG test failures. Out of the 14 failures, eight were found to have failed from subsurface voids or inclusion. The other six failed had crack initiation locations at the material surface. Fig. 11 shows these failed points plotted alongside the $K_S K_R B_{50}^{STB}$ and B_{50}^{RG} curves. It is observed that two distinct populations exist. Four of the six surface failures are over a decade removed from the subsurface failures. It is noted though that two of the surface failures occur very near the subsurface failures. All of the subsurface failures are grouped closely together. Furthermore, the difference in fatigue life between the surface and subsurface groups is visually observed to be approximately equal to the life difference between the $K_S K_R B_{50}^{STB}$ and B_{50}^{RG} curves.

The initiation location factor K_I between the surface and subsurface populations can be defined as the ratio of stresses at the geometric mean lives of subsurface and surface populations corresponding to the SN relationship they originated from:

$$K_I = \frac{\sigma_{max}^{RG} \left[\left(\prod_{i=1}^{f_s} N_{if}^s \right)^{1/f_s} \right]}{\sigma_{max}^{RG} \left[\left(\prod_{i=1}^{f_{ss}} N_{if}^{ss} \right)^{1/f_{ss}} \right]} \tag{12}$$

where f_{ss} and f_s are the numbers of subsurface and surface failures and N_{if}^s and N_{if}^{ss} are individual fatigue lives of subsurface and surface specimens, respectively. This geometric mean lives are plotted on Fig. 11 at the evaluated stress levels forming the ratio in Eq. (13). Eq. (12) results in $K_I = 1.165$ indicating an increase in the STB lives to more closely approximate the RG results. The use of Eq. (12) also assumes that the STB testing resulted in purely sur-

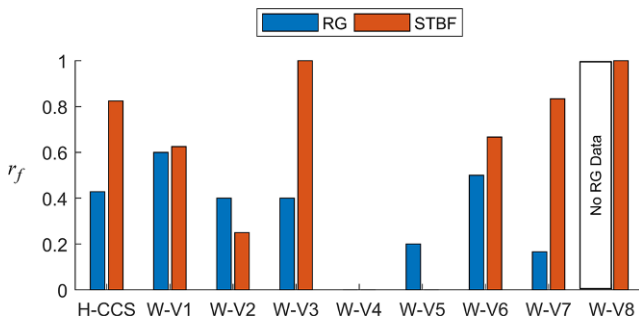


Fig. 12 Comparison of number of surface and subsurface failures for nine different test programs containing STBF and RG data. Data sets W-V1 to W-V8 are from Winkler et al. [2]

face initiated failures. A preliminary fractographic analysis of the STB tests indicates that 14 of 17 failures initiated from surface locations suggesting that the use of Eq. (12) is appropriate.

It might be appropriate to define a ratio of the number of expected surface and subsurface failures found in a single type of testing as

$$r_f = \frac{f_s}{f_s + f_{ss}} \tag{13}$$

Here, a value of r_f approaching 1 indicates that most or all of the failures were surface initiated and a value approaching 0 indicates that most or all of the failure were subsurface initiated. In the tests considered here, $r_f = 0.428$ for the RG testing and $r_f = 0.8235$ for the STB testing. This represents one set of data for one material though it is very desirable to have a larger set as this ratio may be material dependent. The work by Winkler et al. [2] which presented sets of RG and STB testing for eight material variants can be used as a comparison points. Reported surface and subsurface failures for each variant were tabulated and r_f was computed. Fig. 12 shows a comparison of the ratios for each variant used in their testing (W-V1—W-V8) along with the ratios from the testing presented in this research (H-CCS). Six of the nine variants tested with STB methods resulted in a majority or entirely in surface initiated failures. Seven of the eight variants tested by RG methods resulted in a majority or entirely subsurface initiated failures. It is also noteworthy though that two variants tested by STB methods resulted entirely in subsurface initiations. This data review reveals two insights: (i) as a whole, STB testing produces more surface initiated failures and RG produces more subsurface initiated failures, and (ii) this trend can be highly dependent on the material and processing methods. Formulation of the initiation location factor K_I should therefore be done for and material type individually.

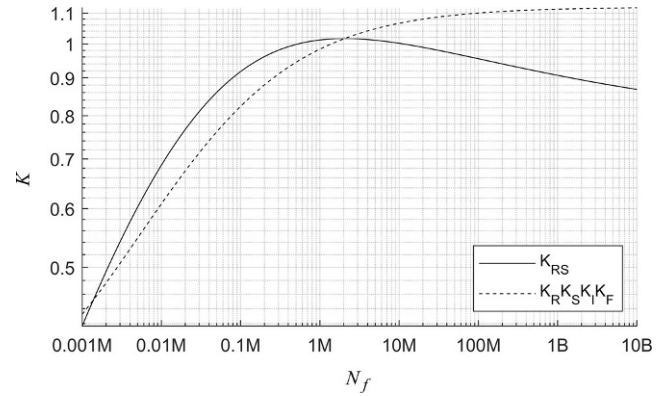


Fig. 13 Comparison of total stress ratio difference between STB and RG testing derived from knowledge of both curves K_{RS} and individually derived ratios from single set data

3.6 Loading factor K_F and remaining differences

The last stress factor discussed is the loading factor K_F , the difference in RG and STB testing due to load waveform variations and test frequencies. Very little is known on this subject and less with respect to gear loading. Experimental studies could be done using STB methodologies but a test machine capable of at least outputting sawtooth or square wave load forms would be needed. Conversely, crack initiation models utilizing simulated root stress time histories from sinusoidal STB testing and RG testing might provide insight into this difference. The methodology described in here may also allow for the extraction of this difference if sufficient confidence is produced for the other three factors and K_F is the only remaining major factor such that

$$K_F = \frac{K_{RS}}{K_S K_R K_I} \tag{14}$$

In this study, $K_F = 1$ as no other data exist to suggest otherwise at this point. The four empirical factors translating STB to RG data or vice versa are then defined using at most one set of gear tooth bending fatigue data per factor.

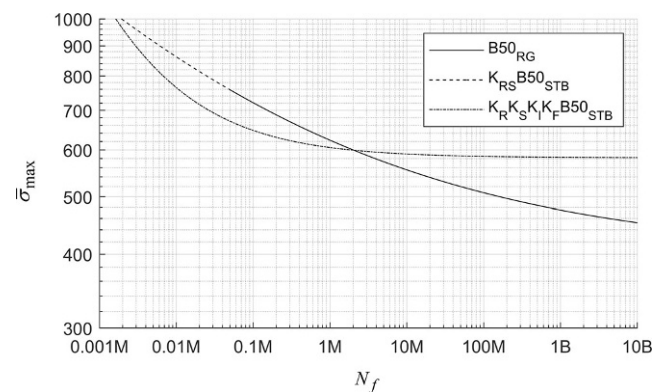


Fig. 14 Comparison of transformed STBF data using the total ratio K_{RS} and the individually derived ratios

The empirical relationship K_{RS} defining the total STB to RG relationship has also been defined. Fig. 13 shows a comparison of K_{RS} defined from both sets of data to $K_F K_S K_R K_I$ derived from single source data sets. A reasonably close agreement is seen, especially in the finite life range below 10M cycles. From there the difference in regressed fatigue strength is shown as $K_F K_S K_R K_I$ fails to predict a lower endurance limit in RG testing. This discrepancy might be due to several reasons including: (i) the regression used does not consider a distribution of fatigue strength between specimens and assumes that one endurance strength exists for all specimens such that the treatment for K_S is nulled, and (ii) the treatment for K_I does not consider any difference in fatigue strength between surface and subsurface failures.

The difference between regressed fatigue strengths is still an unknown, which the current data set cannot define. VHCF data on hourglass specimens suggests that such a fatigue strength occurs at fatigue lives of $(10)^9$ or more, which is beyond the suspension criteria currently used in any typical gear tooth bending fatigue experiment. The regression algorithms used here depended on having suspension data to these levels to determine accurate fatigue strengths. Therefore, it should be seen that the current difference between K_{RS} and $K_F K_S K_R K_I$ at the fatigue strength in this treatment is scrutinized and investigated further. Fig. 14 shows the difference between $K_S K_R K_F K_I B_{50}^{STB}$ and the equivalent $K_{RS} B_{50}^{STB} = B_{50}^{RG}$ curves. The finite life region shows close agreement as with Fig. 13 yet the fatigue strengths diverge as $N_f \rightarrow \infty$.

The error in the estimates used to correlate regressed fatigue strengths stems from the inability of the regression used to develop a variance of the regressed fatigue limit parameter γ with respect to the stress level as well as the possible physical difference in fatigue strengths due to change in surface and subsurface initiation. This could be handled by the inclusion of an addition empirical parameter relating the two fatigue strengths but it is the authors opinion that it would be more prudent to focus on a statistical techniques to first determine what percentage of the difference can be explained statistically. Two techniques exist to regress the fatigue strength as a random variable. The first is sets of up-down data as discussed by Little [47] and the second is to consider the fatigue strength as a random variable within the MLE process as formulated by Pascual and Meeker [48]. Both techniques require data beyond what the test set disclosed in this research contains.

4 Summary and conclusions

Sets of STB and RG tests were presented and analyzed in order to investigate differences in the resulting stress-life relationships. Total difference was accessed via comparison

of the regressed median lives. It was proposed that the total difference is the resultant of four individual differences, namely, the loading factor, stress ratio factor, statistical factor and initiation location factor, and that three of these differences can be accessed directly from a single set of data. Suggested methodologies to extract the ratio of maximum bending stress for equivalent test fatigue lives between STB and RG testing for the stress ratio factor, statistical factor and initiation location factor were described. The difference due to the loading waveform test differences was assumed to be unity as very little information exists on this topic and the resultant three individual factors derived from single set data are compared to the total difference. Moderate agreement was found though the regressed fatigue strengths still differ considerably. This suggests that the proposed treatment either lacks the description of the fatigue strength as another random variable or another empirical conversions factor is needed. As RG testing becomes more accessible, more directly comparable STB and RG test data is needed on additional gear materials to advance current knowledge on this issue to make STB tests more reliable as a design tool.

Funding Not applicable

Declarations

Conflict of interest I. Hong, Z. Teaford and A. Kahraman declare that they have no competing interests.

Ethical standards Ethics approval: Not applicable.

References

1. Yamanaka M, Matsushima Y, Miwa S, Nartta Y, Inoue K, Kawasaki Y (2010) Comparison of bending fatigue strength among spur gears manufactured by various methods: (influence of manufacturing method on bending strength). *J Adv Mech Des Syst Manuf* 4(2):480–491
2. Winkler K, Schurer S, Tobie T, Stahl K (2019) Investigations on the tooth root bending strength and the fatigue fracture characteristics of case-carburized and shot-peened gears of different sizes. *Proc Inst Mech Eng Part C J Mech Eng Sci* 233(21–22):7338–7349
3. Oda S, Shimatomi Y (1980) Study on bending fatigue strength of helical gears (1st report, effect of helix angle on bending fatigue strength). *Bull JSME* 23(177):453–460
4. Oda S, Shimatomi Y (1980) Study on bending fatigue strength of helical gears (2nd report, bending fatigue strength of carehardened helical gears). *Bull JSME* 23(177):461–468
5. Medlin D, Krauss G, Matlock DK, Burris K, Slane M (1995) Comparison of single gear tooth and cantilever beam bending fatigue testing of carburized steel. *SAE Pap*, vol 950212
6. Mcpherson DR, Rao SB (2008) Methodology for translating single-tooth bending fatigue data to be comparable to running gear data. *Gear Technology*: 42–51
7. Krantz T, Tufts B (2008) Pitting and bending fatigue evaluations of a new case-carburized gear steel. *Gear Technol*:863–869. <https://doi.org/10.1115/DETC2007-34090>

8. Kodeeswaran M, Verma A, Suresh R, Senthilvelan S (2016) Bi-directional and uni-directional bending fatigue performance of unreinforced and carbon fiber reinforced polyamide 66 spur gears. *Int J Precis Eng Manuf* 17(8):1025–1033
9. Hohn B-R, Oster P, Tobie T (2003) Systematic investigations on the influence of case depth on the pitting and bending strength of case carburized gears. In: DETC2003/PTG, Chicago, pp 111–119
10. Handschuh RF, Krantz T, Lerch BA, Burke CS (2007) Investigation of low-cycle bending fatigue of AISI 9310 steel spur gears. *NASA TM*, vol 214914
11. Haberer C, Leitner H, Eichseder W, Dietrich A (2009) Fatigue life behavior of a hypoid gear tooth root taking the influences of orbital forging into account. In: SAE World Congress and Exhibition, SAE International
12. Gasparini G, Mariani U, Gorla C, Filippini M, Rosa F (2009) Bending fatigue tests of helicopter case carburized gears: influence of material, design and manufacturing parameters. *Gear Technol* 26(8):68–76
13. Wheatner J, Houser DR (1994) Investigation of the effects of manufacturing variations and materials on fatigue crack detection methods in gear teeth. *NASA CR*, vol 195093
14. Dobler F, Tobie T, Stahl K (2015) Influence of low temperatures on material properties and tooth root bending strength of case-hardened gears. *Proc. ASME Des. Eng. Tech. Conf.*, vol 10
15. Dobler F, Tobie T, Stahl K, Nadolski D, Steinbacher M, Hoffmann F (2016) Influence of hardening pattern, base material and residual stress condition on the tooth root bending strength of induction hardened gears. In: Proceedings of the International Conference on Power Transmissions, pp 287–294
16. Dobler A, Hergesell M, Tobie T, Stahl K (2016) Increased tooth bending strength and pitting load capacity of fine-module gears. *Gear Technol* 33(7):48–53
17. Conrado E, Gorla C, Davoli P, Boniardi M (2017) A comparison of bending fatigue strength of carburized and nitrided gears for industrial applications. *Eng Fail Anal* 78:41–54
18. Blais P, Toubal L (2020) Single-gear-tooth bending fatigue of HDPE reinforced with short natural fiber. *Int J Fatigue* 141:105857
19. Benedetti M, Fontanari V, Höhn BR, Oster P, Tobie T (2002) Influence of shot peening on bending tooth fatigue limit of case hardened gears. *Int J Fatigue* 24(11):1127–1136
20. Wagner M, Isaacson A, Knox K, Hylton T, Wagner M, Isaacson A, Knox K, Hylton T (2020) Single tooth bending fatigue testing at any R ratio. In: AGMA Fall Technical Meeting 20FTM09, pp 1–14
21. Stringer DB, Dykas BD, Laberge KE, Zakrajsek AJ, Handschuh RF (2011) A new high-speed, high-cycle, gear-tooth bending fatigue test capability. *NASA TM*, vol 217039
22. Shen T, Krantz T, Sebastian J (2011) Advanced gear alloys for ultra high strength applications. *NASA TM*, vol 217121
23. Seabrook JB, Dudley DW (1964) Results of a fifteen-year program of flexural fatigue testing of gear teeth. *J Eng Ind* 86(3):221–237
24. Savaria V, Bridier F, Bocher P (2016) Predicting the effects of material properties gradient and residual stresses on the bending fatigue strength of induction hardened aeronautical gears. *Int J Fatigue* 85:70–84
25. Sanders A, Houser DR, Kahraman A, Harianto J, Shon S (2011) An experimental investigation of the effect of tooth asymmetry and tooth root shape on root stresses and single tooth bending fatigue life of gear teeth. In: ASME International Power Transmission and Gearing Conference, Washington D.C.
26. SAE International Surface Vehicle Recommended Practice (1997) Single tooth gear bending fatigue test. *SAE Stand*, vol J1619
27. Rao SB, Mcpherson DR (2003) Experimental characterization of bending fatigue strength in gear teeth. *Gear Technol* 20:25–32
28. Phelan PE, Sell DJ, Dowling WE (1996) Bending fatigue behavior of carburized gear steels: planetary gear test development and evaluation. *SAE Pap*, vol 960978
29. Hong IJ, Kahraman A, Anderson N (2020) A rotating gear test methodology for evaluation of high-cycle tooth bending fatigue lives under fully reversed and fully released loading conditions. *Int J Fatigue* 133:105432
30. Hong IJ, Kahraman A, Anderson N (2021) An experimental evaluation of high-cycle gear tooth bending fatigue lives under fully reversed and fully released loading conditions with application to planetary gear sets. *J Mech Des* 143(2):1–9
31. Hatano A, Namiki K (1992) Application of hard shot peening to automotive transmission gears. *SAE Pap*, vol 938179
32. Hasl C, Illenberger C, Oster P, Tobie T, Stahl K (2018) Potential of oil-lubricated cylindrical plastic gears. *J Adv Mech Des Syst Manuf* 12(1):1–9
33. Hong IJ, Kahraman A, Anderson N (2020) An experimental evaluation of high-cycle gear tooth bending fatigue lives under fully reversed and fully released loading conditions with application to planetary gear sets. *J Mech Des* 143(2). <https://doi.org/10.1115/1.4047687>
34. Selines RJ (1972) Effect of cyclic stress wave form on corrosion fatigue crack propagation in Al-Zn-Mg alloys. *Met Trans* 3(9):2525–2531
35. Menan F, Henaff G (2009) Influence of frequency and exposure to a saline solution on the corrosion fatigue crack growth behavior of the aluminum alloy 2024. *Int J Fatigue* 31(11–12):1684–1695
36. Müller G (1873) Zulässige Inanspruchnahme Des Schmiedeeisens Bei Brückenkonstruktionen. *Z Österr Ing Archit* 25:197–202
37. Sendeckyj GP (2001) Constant life diagrams—A historical review. *Int J Fatigue* 23(4):347–353
38. Novovic D, Dewes RC, Aspinwall DK, Voice W, Bowen P (2004) The effect of machined topography and integrity on fatigue life. *Int J Mach Tools Manuf* 44(2–3):125–134
39. Murakami Y (2002) Metal fatigue: effects of small defects and non-metallic inclusions
40. Nakajima M, Tokaji K, Itoga H, Ko HN (2003) Morphology of step-wise S-N curves depending on work-hardened layer and humidity in a high-strength steel. *Fatigue Fract Eng Mater Struct* 26(12):1113–1118
41. Stahl K (1999) Statistische Methoden Zur Beurteilung von Bauteillebensdauer Und Zuverlässigkeit Und Ihre Beispielhafte Anwendung Auf Zahnräder. *FVA-Forschungsvorhaben*, vol 304. Forschungsvereinigung Antriebstechnik, Frankfurt
42. Rettig H (1987) Ermittlung von Zahnfußfestigkeitskennwerten Auf Verspannungsprüfständen Und Pulsatoren-Vergleich Der Prüfverfahren Und Der Gewonnenen Kennwerte. *Antriebstechnik* 26:51–55
43. Pyttel B, Schwerdt D, Berger C (2011) Very high cycle fatigue—Is there a fatigue limit? *Int J Fatigue* 33(1):49–58
44. The Gear and Power Transmission (2021) Research Laboratory Windows-LDP, load distribution program. The Ohio State University, Columbus
45. Pascual FG, Meeker WQ (1997) Analysis of fatigue data with runouts based on a model with nonconstant standard deviation and a fatigue limit parameter. *J Test Eval* 25(3):292–301
46. Sutherland H, Veers P (2000) The development of confidence limits for fatigue strength data. In: 2000 ASME Wind Energy Symposium, pp 1–11
47. Little RE (1990) Optimal stress amplitude selection in estimating median fatigue limits using small samples. *J Test Eval* 18(2):115–122
48. Pascual FG (2003) A standardized form of the random fatigue-limit model. *Commun Stat Part B Simul Comput* 32(4):1205–1221